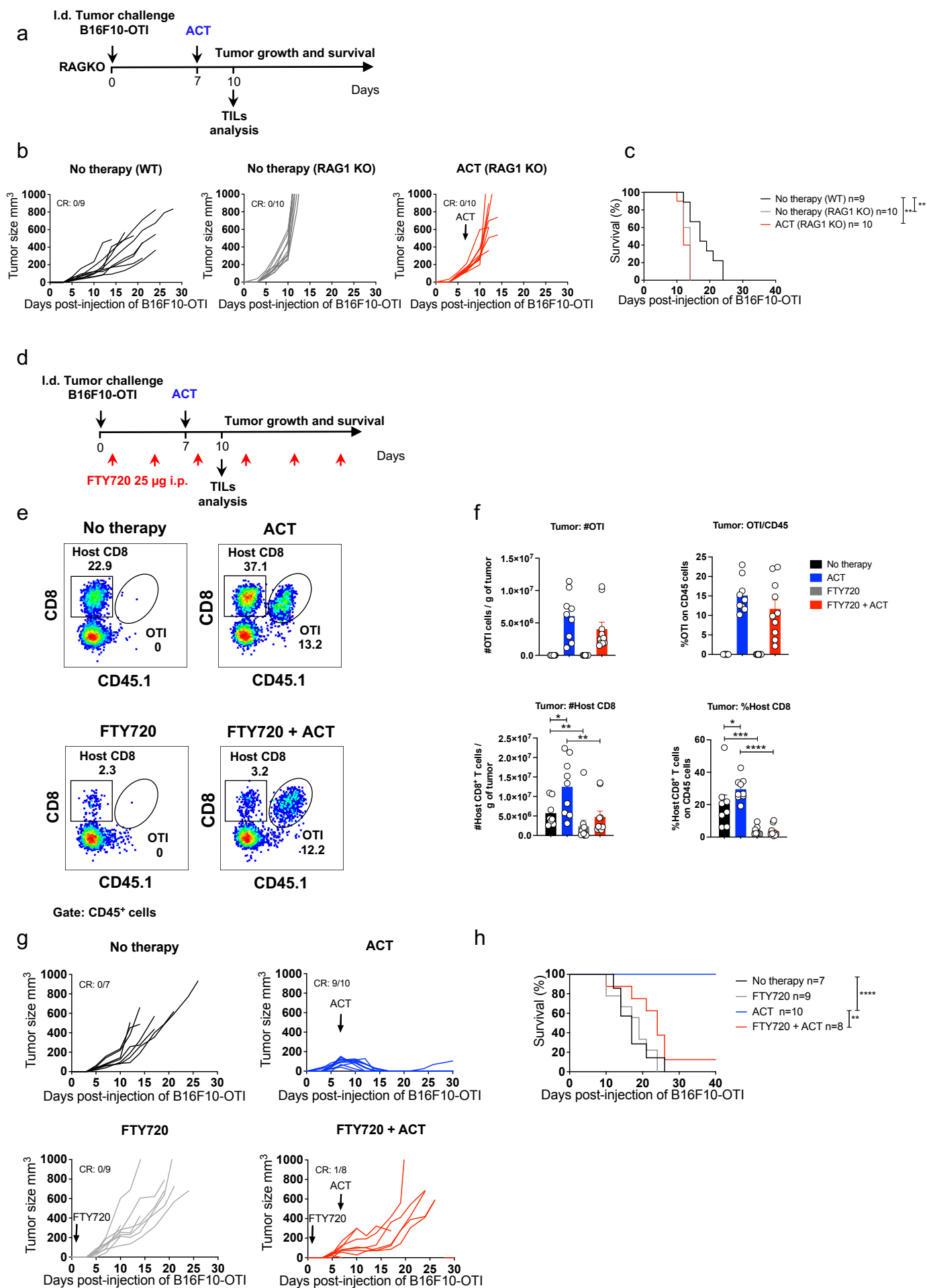
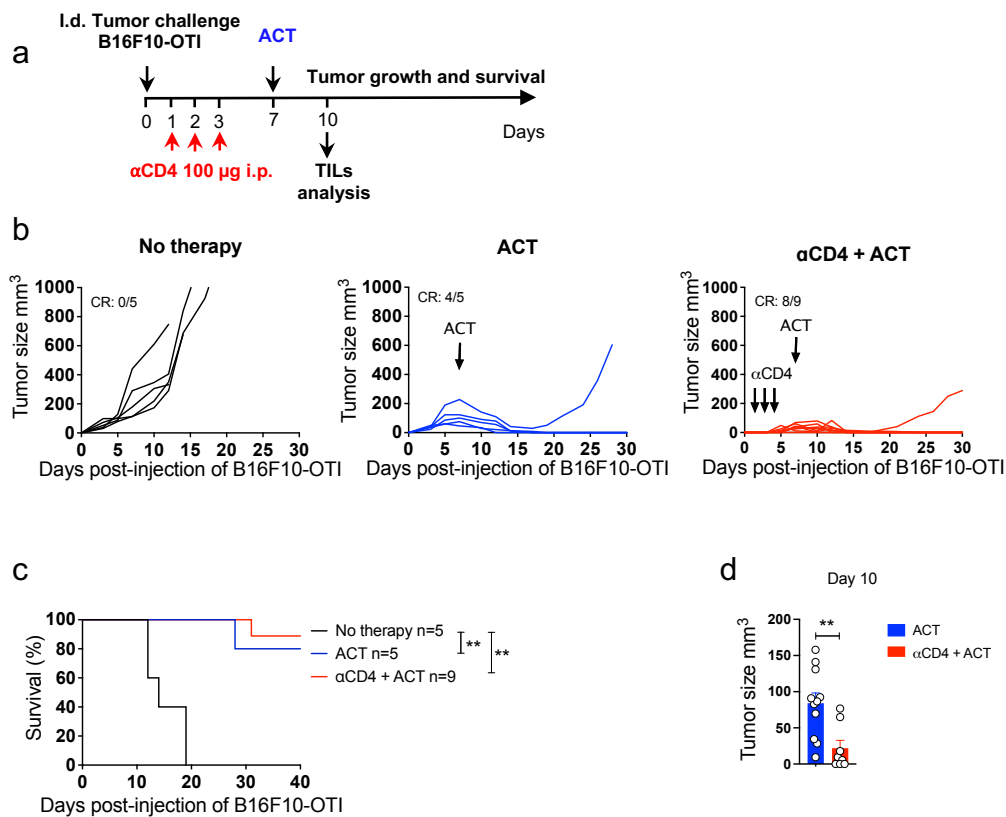


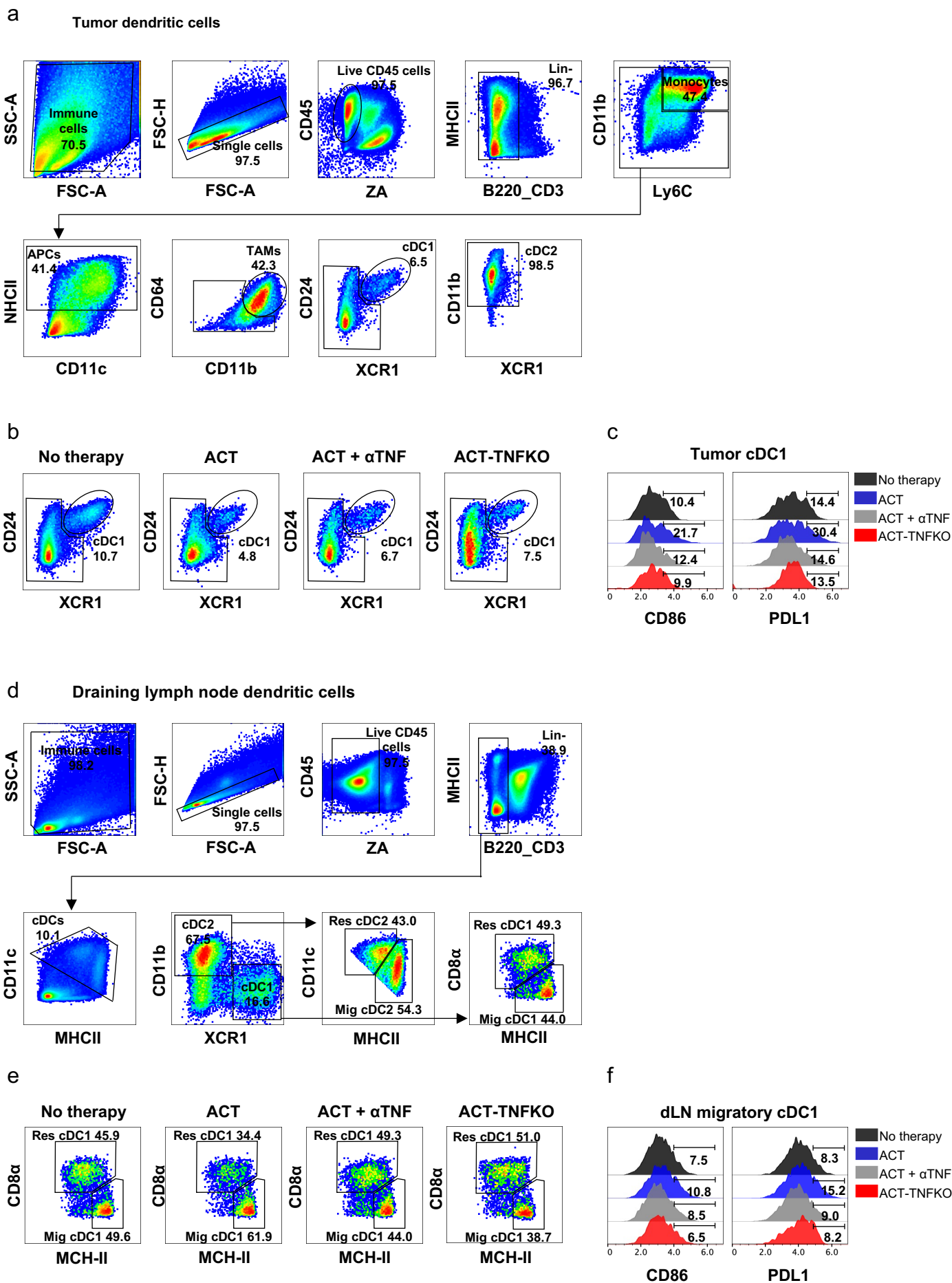
Supplementary Figure 1. Suboptimal ACT does not promote tumor accumulation of host CD8⁺ T cells, leading to tumor progression. C57BL/6 mice bearing B16F10-OTI tumors received i.v. transfer of 0.5×10^6 *in vitro* activated OTI CD8⁺ T cells as a Suboptimal ACT. Untreated mice (No therapy) were used as controls. **a** Experimental scheme. **b-c** Individual tumor growth (**b**) and Kaplan-Meier (**c**) curves for each group: No therapy (black curves) and Suboptimal ACT (red curves). **d-e** Tumor infiltrates were analyzed by flow cytometry three days after ACT. **d** Left panels: Representative dot plots displaying the frequencies of host (square, CD45.1⁻) and transferred (ellipse, OTI CD45.1⁺) CD8⁺ T cells in live CD45⁺ cells. Middle and right panels: Representative dot plots displaying the expression of PD-1 and granzyme B in host (middle) and transferred (right) CD8⁺ T cells and the frequencies of the different subpopulations defined in each quadrant: PD-1⁺GzmB⁻, PD-1⁺GzmB⁺, PD-1⁻GzmB⁻ and PD-1⁻GzmB⁺. **e** Quantifications of CD45⁺ cells as a percentage of total live cells, transferred OTI, total host CD8⁺ T cells and their PD-1⁺ GzmB⁻ and PD-1⁺ GzmB⁺ subsets as a percentage of CD45⁺ cells. (**c**) Kaplan-Meier curves show survival from two independent experiments. Statistical significance was assessed using two-sided log-rank Mantel-Cox test * $P < 0.05$. (**e**) Pooled data from two independent experiments, No therapy $n = 12$; Suboptimal ACT $n = 12$. Bars represent mean \pm SEM. Statistical significance was assessed using two-sided unpaired Mann-Whitney test **** $P < 0.0001$. CR = Complete Response.



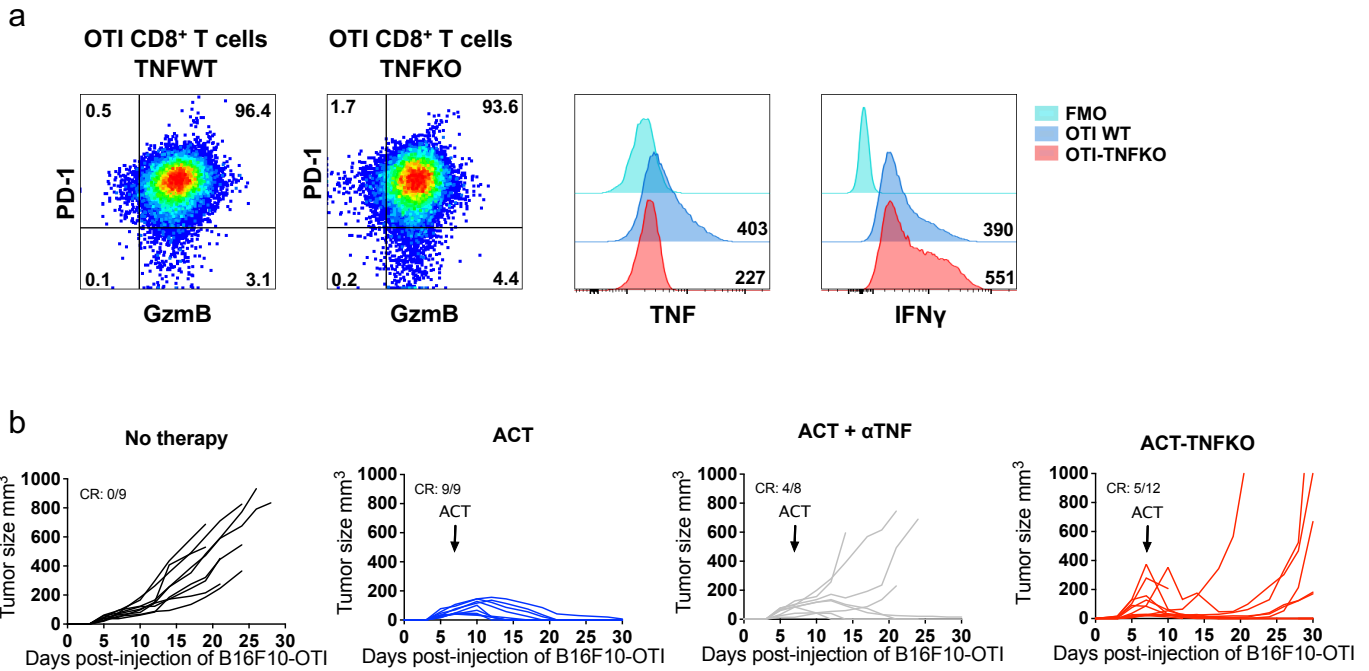
Supplementary Figure 2. Host T cells are required for ACT-induced tumor eradication. a-c RAG1 KO mice bearing B16F10-OTI tumors received i.v. transfer of 1×10^6 in vitro activated OTI CD8⁺ T cells (ACT). WT C57BL/6 untreated mice (No therapy) were used as controls. **a** Experimental timeline. **b-c** Individual tumor growth (**b**) and Kaplan-Meier (**c**) curves for each group: No therapy WT mice (black curves), No therapy RAG1 KO mice (grey curves), and ACT RAG1 KO mice (red curves). **d-h** C57BL/6 mice bearing B16F10-OTI tumors received i.p. injections of FTY720 every three days starting one day after the tumor challenge. Mice were i.v. transferred with 1×10^6 in vitro activated OTI CD8⁺ T cells (ACT). **d** Experimental scheme. **e-f** Tumor infiltrating lymphocytes were analyzed by flow cytometry three days after ACT. **e** Representative dot plots displaying the frequencies of host (square, CD45.1⁻) and transferred (ellipse, OTI CD45.1⁺) CD8⁺ T cells within live CD45⁺ cells for each group: No therapy, ACT, No therapy + FTY720, and ACT + FTY720. **f** Absolute quantifications (cells/g tumor) and relative (on CD45⁺ cells) of transferred OTI (upper panel) and host (lower panel) CD8⁺ T cells for each group: No therapy (black bars), ACT (blue bars), No therapy + FTY720 (grey bars), ACT + FTY720 (red bars). **g-h** Individual tumor growth (**g**) and Kaplan-Meier (**h**) curves for each group: No therapy (black curves), ACT (blue curves), No therapy + FTY720 (gray curves), ACT + FTY720 (red curves). (**c**) Results from two independent experiments. Statistical significance was assessed using two-sided log-rank Mantel-Cox test ** $P < 0.01$, *** $P < 0.001$. (**f**) Pooled data from two independent experiments, No therapy $n=8$, ACT $n=9$, No therapy + FTY720 $n=10$, and ACT + FTY720 $n=10$. Bars are the mean \pm SEM. Statistical significance was assessed using two-sided unpaired Mann-Whitney test * $P < 0.05$, ** $P < 0.01$, *** $P < 0.001$, **** $P < 0.0001$. (**h**) Results from two independent experiments. Statistical significance was assessed using two-sided log-rank Mantel-Cox test. * $P < 0.05$, **** $P < 0.0001$. CR = Complete Response; TP = Total Protection.



Supplementary Figure 3. CD4⁺ T cell depletion does not affect ACT-mediated tumor eradication. C57BL/6 mice bearing B16F10-OTI tumors received i.v. transfer of 1×10^6 in vitro activated OTI CD8⁺ T cells (ACT). A group of mice received three i.p. daily doses of αCD4 antibody starting one day after tumor challenge. Untreated mice (No therapy) were used as controls. **a** Experimental timeline. **b-c** Individual tumor growth (**b**) and Kaplan-Meier (**c**) curves for each group: No therapy (black curves), ACT (blue curves), αCD4 + ACT (red curves). **d** day 10 tumor size quantification (**c**) Results from two independent experiments. Statistical significance was assessed using two-sided log-rank Mantel-Cox test $**P < 0.01$. (**d**) Pooled data from two independent experiments, ACT n=11; αCD4 + ACT n=8. Bars are the mean \pm SEM. Statistical significance was assessed using two-sided unpaired Mann-Whitney test $**P < 0.01$. CR = Complete Response.

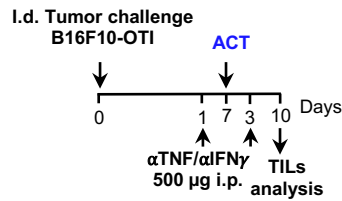


Supplementary Figure 4. Dendritic cell analysis by flow cytometry in tumors and draining lymph nodes. CD45⁺ cells from tumor and draining lymph node of B16F10-OTI melanoma tumors bearing mice were isolated and stained for flow cytometry analysis. **a-b** Analysis of tumor-infiltrating DCs. Gating strategy to define cDC1 and cDC2. **b** Representative dot-plots showing the expression of CD24 and XCR1 within DC population (Lin⁻CD11c⁺MHCII⁺) of each group: No therapy, ACT, ACT + TNF and ACT-TNFKO. **c** Representative histograms showing normalized expression of CD86 and PDL1 in cDC1. **d-e** Analysis of DCs in draining lymph nodes. **d** Gating strategy to define lymph node-resident and migratory cDC1 and cDC2. **e** Representative dot-plots of each group: No therapy, ACT, ACT + TNF and ACT-TNFKO. **f** Representative histograms showing the normalized expression of CD86 and PDL1 in migratory cDC1.

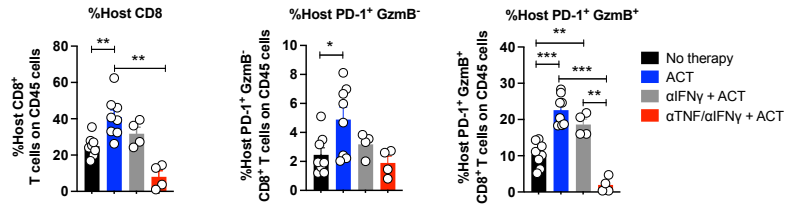


Supplementary Figure 5. Effector phenotype and *in vivo* antitumor activity of WT and TNF-KO OTI CD8⁺ T cells. **a** In vitro activated WT and TNFKO OTI CD8⁺ T cells were reactivated with OTI peptide in the presence of brefeldin A to analyze intracellular TNF and IFN γ production. Representative dot plots showing the expression of PD-1 and GzmB (Left panels). Representative histograms showing the expression of TNF and IFN γ by flow cytometry of WT and TNFKO CD8⁺ T cells. **b-c** C57BL/6 mice bearing B16F10-OTI tumors received i.v. transfer of 1×10^6 in vitro activated WT (ACT) or TNFKO (ACT-TNFKO) OTI CD8⁺ T cells. **b** Individual tumor growth curves of each group: No therapy (black curves), ACT (blue curves), ACT + α TNF (gray curves) and ACT-TNFKO (red curves). **c** Mice that eliminated primary tumors following ACT or ACT-TNFKO were rechallenged with wild-type B16F10 cells in the opposite flank. Individual tumor growth curves of each group: Control (black curves), ACT (blue curves), and ACT-TNFKO (red curves). CR = Complete Response.

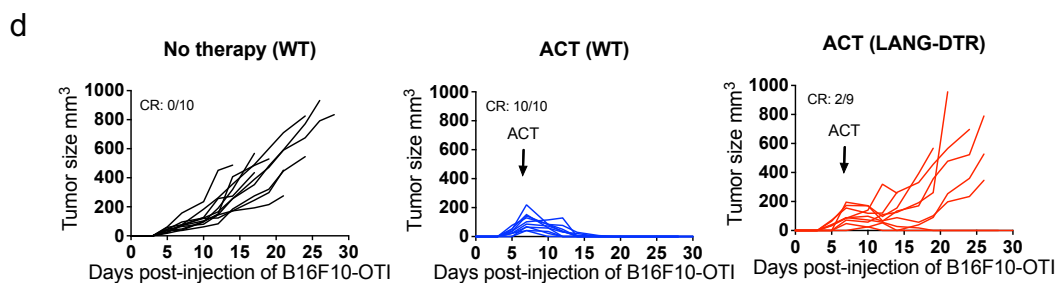
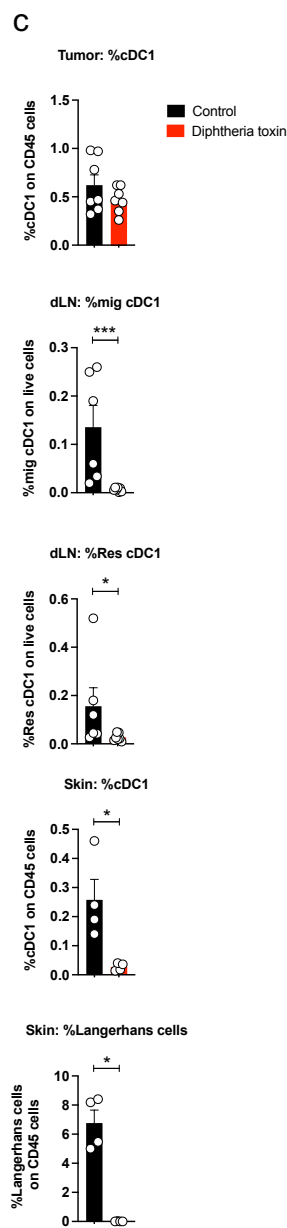
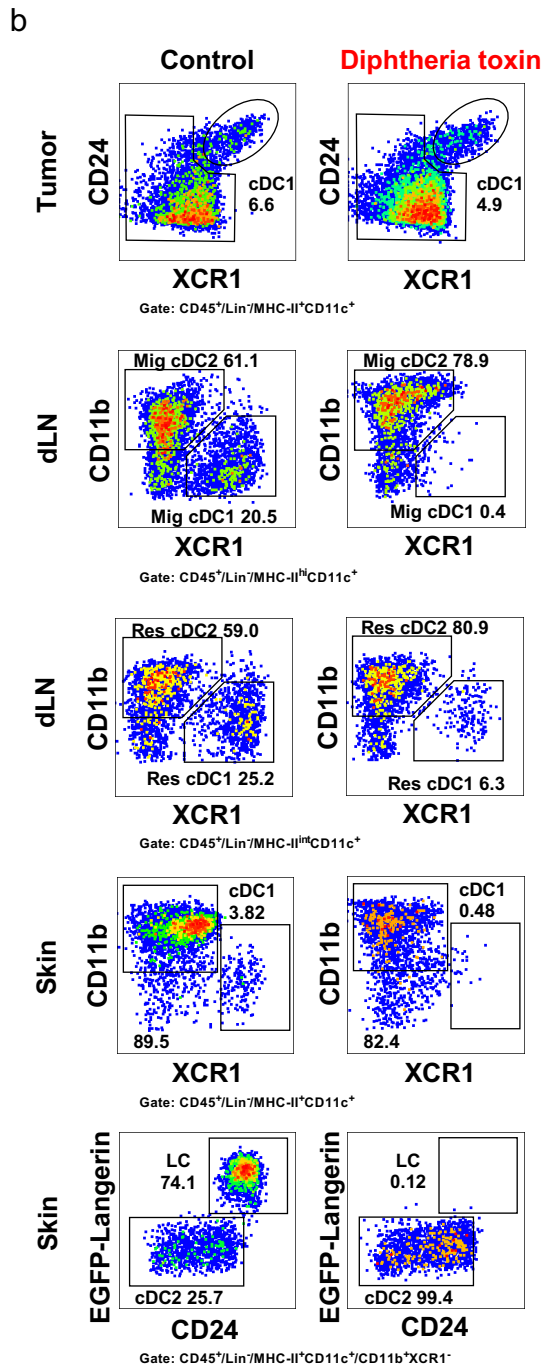
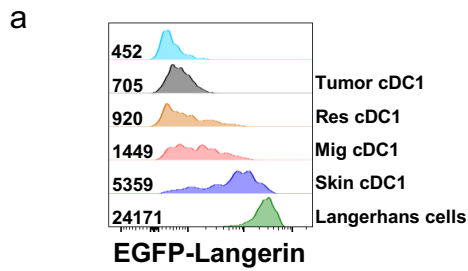
a



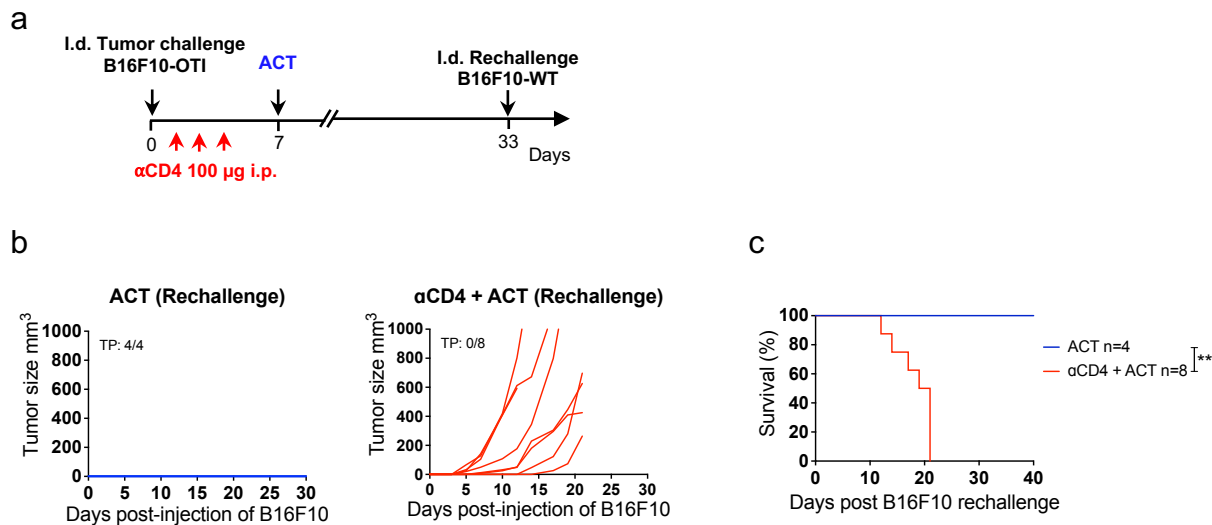
b



Supplementary Figure 6. IFN γ blockade does not affect ACT-induced tumor accumulation of host CD8⁺ T cells. **a-b** C57BL/6 mice bearing B16F10-OTI tumors received i.v. transfer of 1×10^6 in vitro activated OTI CD8⁺ T cells (ACT). Mice also received α IFN γ antibody i.p. alone or in combination with α TNF every other day starting one day before ACT. Tumor infiltrating lymphocytes were analyzed by flow cytometry three days after ACT. **a** Experimental design. **b** Relative quantification of host CD8⁺ T cells and their PD-1⁺ GzmB⁻ and PD-1⁺ GzmB⁺ subpopulation on CD45⁺ cells. (**b**) Data from two independent experiments, No therapy n=8; ACT n=8; α IFN γ + ACT n=4; α TNF/ α IFN γ + ACT n=4. Bars are the mean \pm SEM. Statistical significance was assessed using two-sided unpaired Mann-Whitney test *P<0.05, **P<0.01, ***P<0.001, ****P<0.0001.

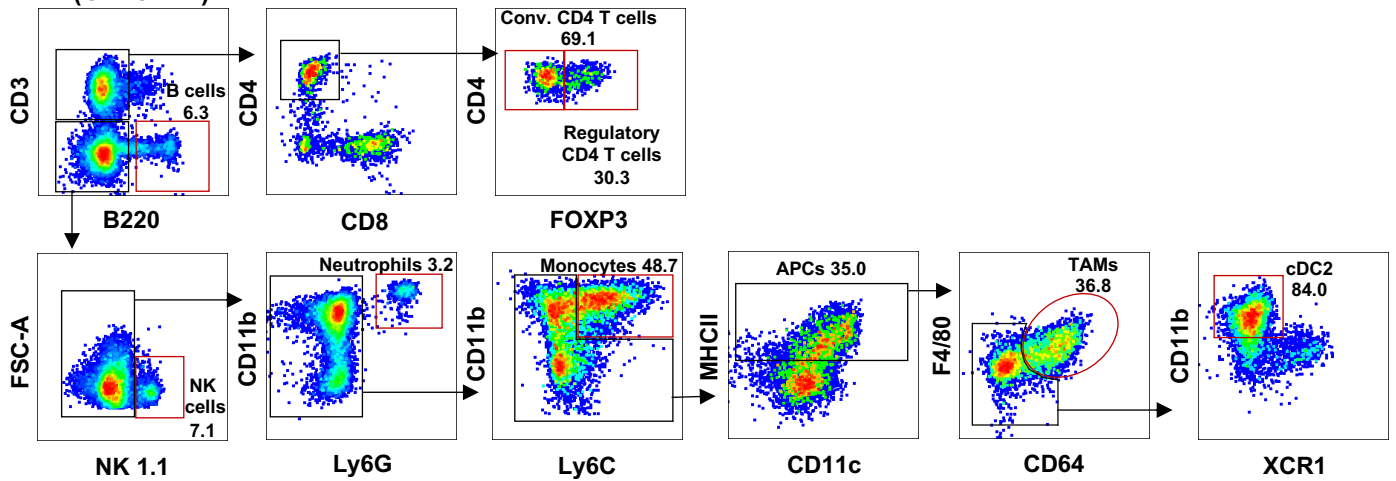


Supplementary Figure 7. Dendritic cell analysis and ACT-induced antitumor efficacy in Langerin-DTR mice. Lang-DTR mice bearing B16F10-OTI tumors were processed to analyze EGFP-langerin expressing DCs from tumor, skin and draining lymph node as well as Langerhans cells from skin. **a** Representative histograms showing the expression of EGFP-Langerin in cDC1 across different tissues and Langerhans cells from skin. **b** Mice receiving i.v. 1 µg of diphtheria toxin or control vehicle were analyzed three days later. Representative dot-plots showing frequencies of cDC1 and Langerhans cells in the different tissues. **c** Quantifications of: cDC1 in tumors; migratory and resident cDC1 in draining lymph nodes; cDC1 and Langerhans cells in skin. **d** Individual tumor growth curves of WT and LANG-DTR mice treated with ACT: No therapy in WT (black curves), ACT in WT (blue curves), and ACT in LANG-DTR (red curves). **(c)** Tumor: Pool of two independent experiments, Control n=7; Diphtheria toxin n=7. dLN: Pool of two independent experiments, Control n=6; Diphtheria toxin n=6. Skin: One experiment, Control n=4; Diphtheria toxin n=4. Bars are the mean ± SEM. Statistical significance was assessed using two-sided unpaired Mann–Whitney test *P<0.05, ***P<0.001.

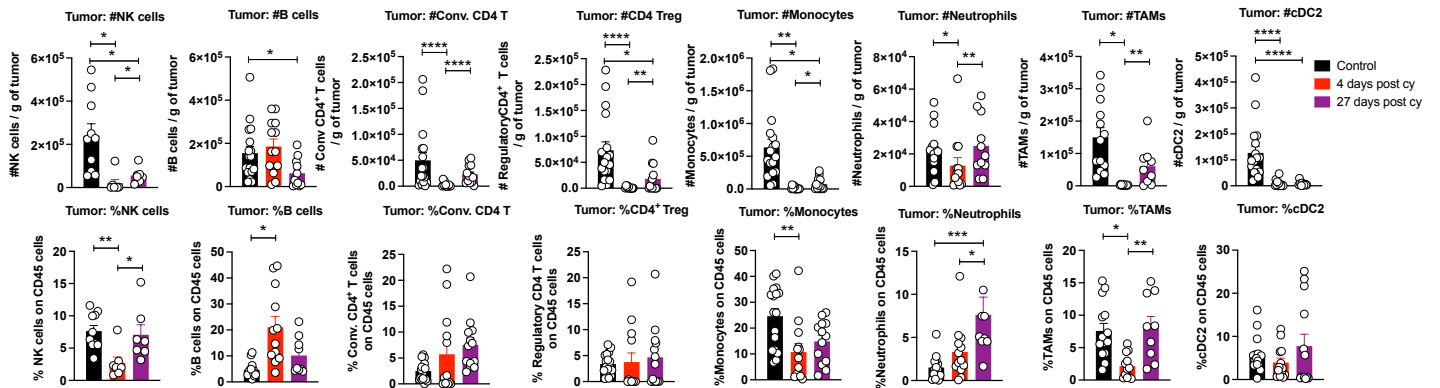


Supplementary Figure 8. CD4⁺ T cell depletion prior to ACT-mediated primary tumor elimination abolishes protection against rechallenge with ACT-resistant tumor cells. C57BL/6 mice bearing B16F10-OTI tumors received three i.p. daily doses of α CD4 antibody starting one day after tumor challenge, then 1×10^6 in vitro activated OTI CD8⁺ T cells (ACT) were administrated by i.v. injection. Mice that eliminated primary tumors following ACT were rechallenged with 1×10^6 wild-type B16F10 cells. **a** Experimental timeline. **b,c** Individual tumor growth (**b**) and Kaplan-Meier (**c**) curves of rechallenged groups: ACT (blue curves), α CD4 + ACT. (**c**) Results from two independent experiments. Statistical significance was assessed using two-sided log-rank Mantel-Cox test. ** $P < 0.01$. TP = Total Protection.

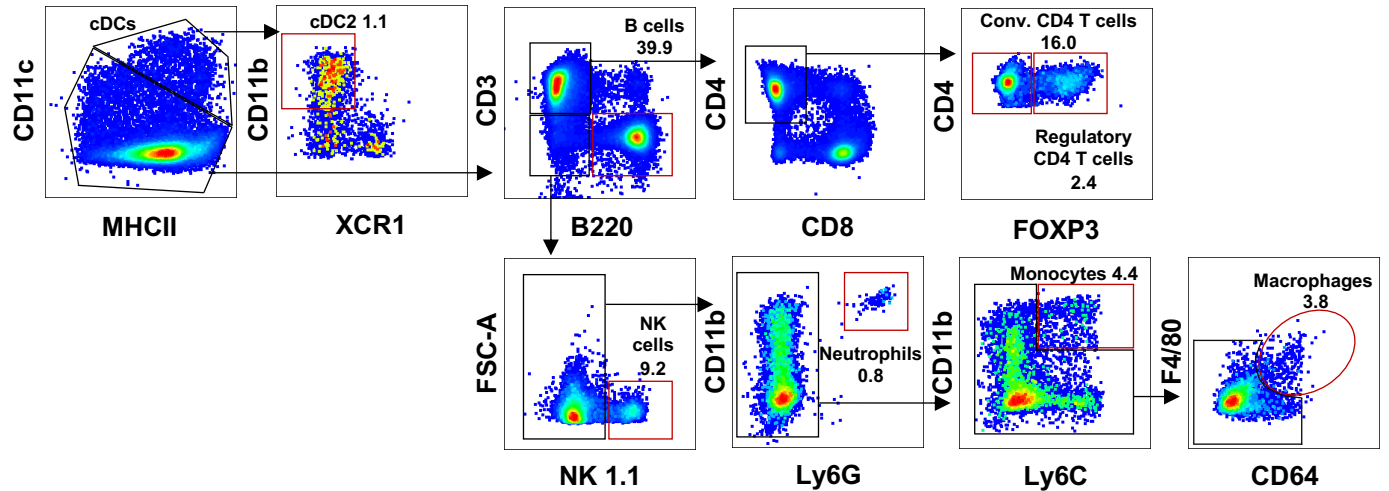
a Live CD45 cells (CD45⁺ZA⁻)



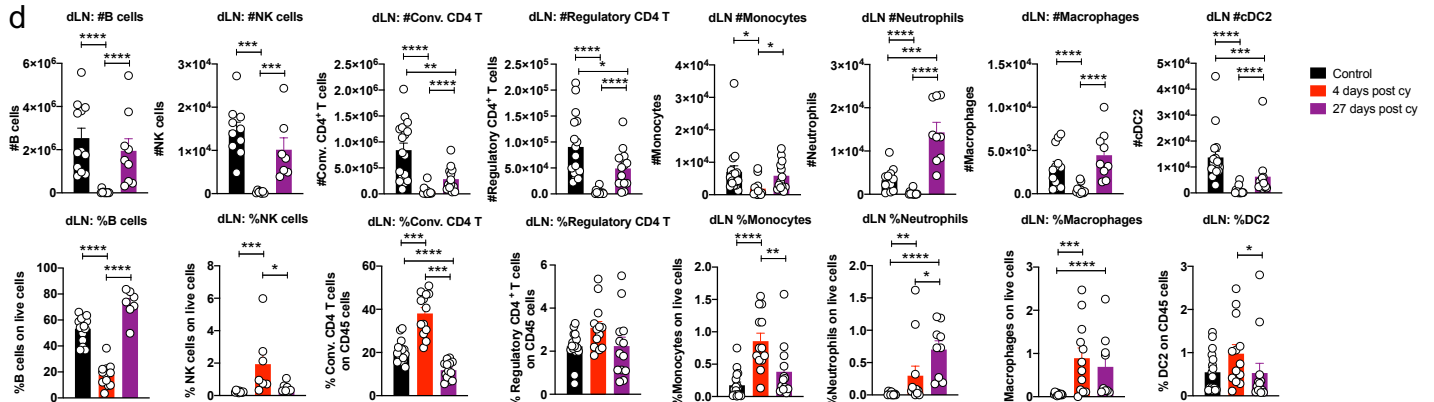
b



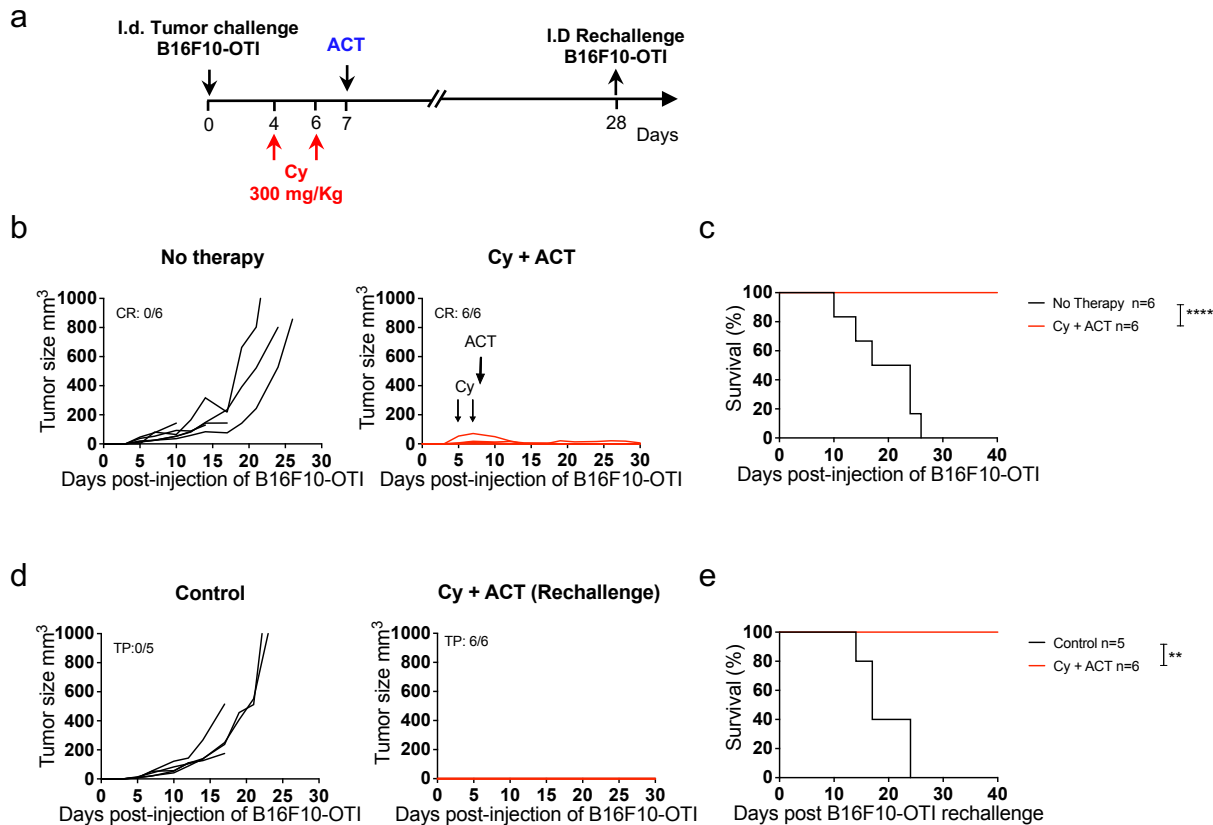
c Live CD45 cells (CD45⁺ZA⁻)



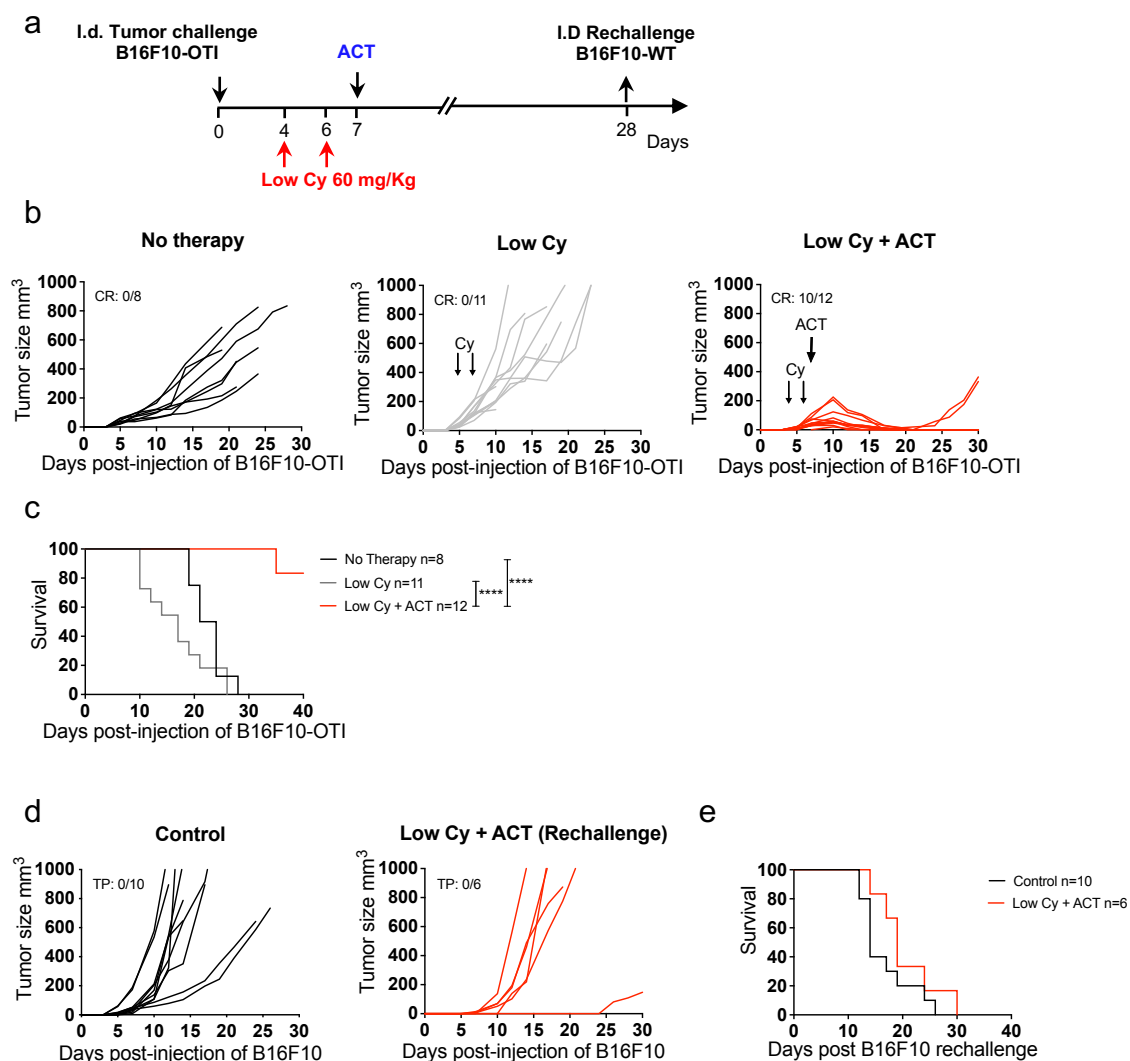
d



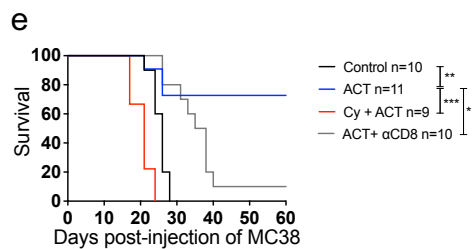
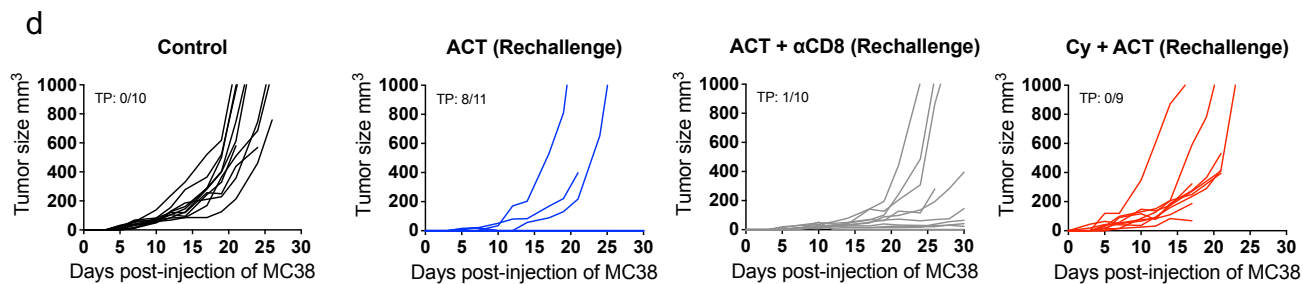
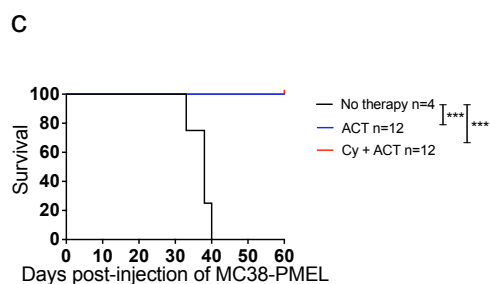
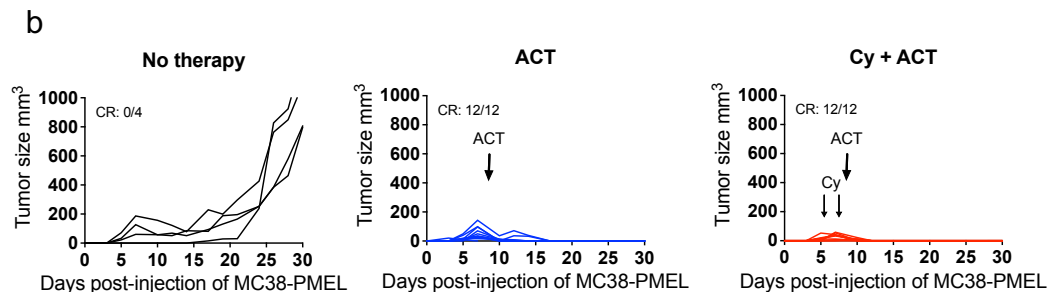
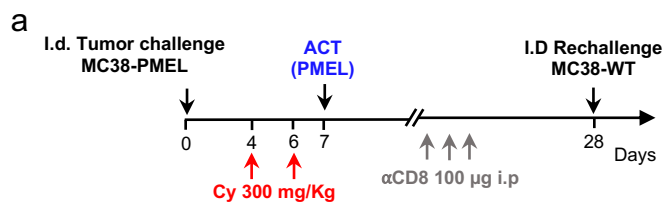
Supplementary Figure 9. Cyclophosphamide preconditioning effects on NK cells, B cells, myeloid cells and CD4⁺ T cell subsets in tumors and draining lymph nodes. C57BL/6 mice bearing B16F10-OTI tumors received i.p. administration of cyclophosphamide (Cy, 300 mg/kg) on days 4 and 6 post-tumor challenge. Tumors and draining lymph nodes were analyzed at 4 and 27 days post-treatment. **a-b** Flow cytometry analysis of tumors infiltrating immune cells **a** Representative dot plots showing gating strategies on live CD45⁺ cells for NK cells, B cells, neutrophils, monocytes, tumor-associated macrophages (TAMs), cDC2 and conventional CD4⁺ and regulatory CD4⁺ T cell subsets highlighted in red squares. **b** Absolute (cells/g) and relative (frequency among CD45⁺ cells) quantifications of NK cells, B cells, neutrophils, monocytes, TAMs, cDC2 and conventional CD4⁺ and regulatory CD4⁺ T cell subsets. **c-d** Flow cytometry analysis of draining lymph nodes. **c** Representative dot plots showing gating strategies for NK cells, B cells, neutrophils, monocytes, macrophages, cDC2 and conventional CD4⁺ and regulatory CD4⁺ T cell subsets. **d** Absolute (cells/g) and relative (frequency among CD45⁺ cells) quantifications of NK cells, B cells, neutrophils, monocytes, macrophages, cDC2 and conventional CD4⁺ and regulatory CD4⁺ T cell subsets. Data in (b, d) are pooled from five independent experiments, Control n =17; 4 days post cy n=13; 27 days post cy n=13. Bars represent mean \pm SEM. Statistical significance was assessed using two-sided unpaired Mann-Whitney test *P<0.05, **P<0.01, ***P<0.001, ****P<0.0001.



Supplementary Figure 10. Long-term protection against ACT-targeted antigen is maintained in lymphodepleted mice. **a-e** C57BL/6 mice bearing B16F10-OTI tumors received 300 mg/kg cyclophosphamide (Cy) i.p. on days 4 and 6 after tumor challenge as a preconditioning lymphodepleting regimen. One day later, mice received i.v. transfer of 1×10^6 *in vitro* activated OTI CD8⁺ T cells. Mice that rejected primary tumors following Cy + ACT were rechallenged with B16F10-OTI cells in the opposite flank. **a** Experimental scheme **b-c** Individual tumor growth (**b**) and Kaplan-Meier (**c**) curves for each condition: No therapy (black curves) and Cy + ACT (red curves). **d-e** Individual tumor growth (**d**) and Kaplan-Meier (**e**) curves of rechallenged mice: Control (black curves) and Cy + ACT (red curves) (**c, e**) Results from one experiment. Statistical significance was assessed using two-sided log-rank Mantel-Cox test ** $P < 0.01$, **** $P < 0.0001$. CR = Complete Response; TP = Total Protection.

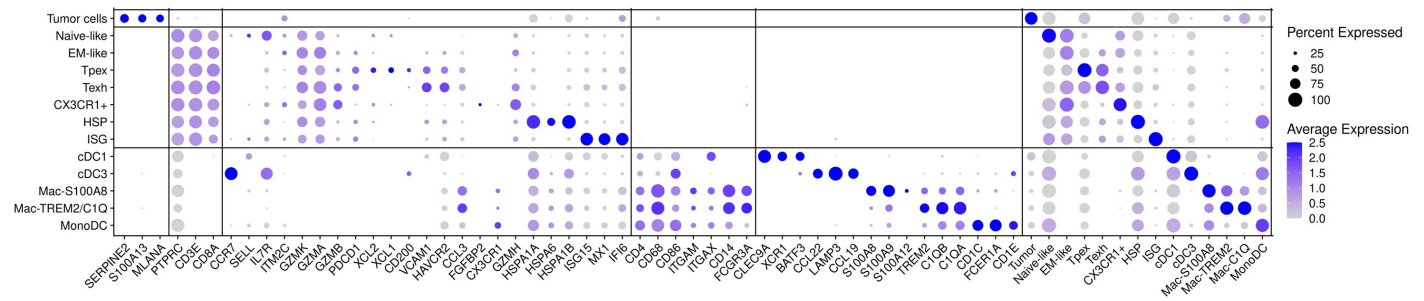


Supplementary Figure 11. Lymphodepleting preconditioning with low dose cyclophosphamide abrogates protection against ACT-resistant tumor cells. C57BL/6 mice bearing B16F10-OTI tumors received 60 mg/kg cyclophosphamide (Cy) i.p. on days 4 and 6 after tumor challenge as a preconditioning lymphodepleting regimen. One day later mice received i.v. transfer of 1×10^6 *in vitro* activated OTI CD8⁺ T cells. **a** Experimental scheme **b-c** Individual tumor growth (**b**) and Kaplan-Meier (**c**) curves for each group: No therapy (black curves), Low Cy (gray curves) and Low Cy + ACT (red curves). **d-e** Mice that eliminated primary tumors following Low Cy ACT were rechallenged with wild-type B16F10 cells in the opposite flank. Individual tumor growth (**d**) and Kaplan-Meier (**e**) curves of Control (black curves) and Low Cy + ACT mice (red curves). (**c**, **e**) Results from two independent experiments. Statistical significance was assessed using two-sided log-rank Mantel-Cox test ****P<0.0001. CR = Complete Response; TP = Total Protection.



Supplementary Figure 12. PMEL-1 ACT eliminates MC38-PMEL tumors and confers host CD8⁺ T cell-mediated protection against ACT-resistant tumor cells that is abrogated by lymphodepleting preconditioning. C57BL/6 mice bearing MC38-PMEL tumors received 300 mg/kg cyclophosphamide (Cy) i.p. on days 4 and 6 after tumor challenge as lymphodepleting preconditioning regimen. One day later, mice received i.v. transfer of 1×10^6 *in vitro* activated PMEL CD8⁺ T cells (ACT). Untreated mice (No therapy) were used as controls. Some ACT-treated mice that rejected tumors received three doses of α CD8 before rechallenge. **a** Experimental scheme. **b-c** Individual tumor growth (**b**) and Kaplan-Meier (**c**) curves for each group: No therapy (black curves), and ACT (blue curves) and Cy + ACT (red curves). **d-e** Mice that rejected primary tumors following ACT or Cy + ACT were challenged with MC38 cells in the opposite flank. A group of mice treated with ACT received three i.p. daily doses of α CD8 antibodies prior to rechallenge. Individual tumor growth (**d**) and Kaplan-Meier (**e**) curves for rechallenged group: Control (black curves), ACT (blue curves), ACT + α CD8 (gray curves) and Cy + ACT (red curves). (**c**) Results from two independent experiments. Statistical significance was assessed using two-sided log-rank Mantel-Cox test *** $P < 0.001$. (**e**) Results from two independent experiments. Statistical significance was assessed using two-sided log-rank Mantel-Cox test. * $P < 0.05$, ** $P < 0.01$, *** $P < 0.001$. CR = Complete Response; TP = Total Protection.

a



Supplementary Figure 13. Cell type annotation of tumor and immune clusters identified by scRNA-seq in TIL-treated melanoma patients. a Dot plot showing average gene expression (color scale) and percentage of cells expressing each gene (dot size) across the major cell clusters identified in the UMAP analysis (Fig. 7b). Marker genes were selected to annotate Tpex, Tex, cDC1, cDC2, monocyte-derived cells, and tumor cells based on established lineage and functional markers. This analysis was used to annotate clusters in Figure 6b and to define gene signatures for downstream functional and clinical correlation analyses.